

Delocalized Electronic Excitations and their Role in Directional Charge Transfer in the Reaction Center of *Rhodobacter Sphaeroides*

Sabrina Volpert,¹ Zohreh Hashemi,¹ Johannes M. Foerster,¹ Mario R. G. Marques,¹ Ingo Schelter,¹ Stephan Kümmel,¹ and Linn Leppert^{2,1}

¹*Institute of Physics, University of Bayreuth, 95440 Bayreuth, Germany*

²*MESA+ Institute for Nanotechnology, University of Twente, 7500 AE Enschede, The Netherlands*

(*Electronic mail: l.leppert@utwente.nl)

(Dated: 26 December 2022)

In purple bacteria, the fundamental charge-separation step that drives the conversion of radiation energy into chemical energy proceeds along one branch - the A branch - of a heterodimeric pigment-protein complex, the reaction center. Here, we use first principles time-dependent density functional theory (TDDFT) with an optimally-tuned range-separated hybrid functional to investigate the electronic and excited-state structure of the primary six pigments in the reaction center of *Rhodobacter sphaeroides*. By explicitly including amino-acid residues surrounding these six pigments in our TDDFT calculations, we systematically study the effect of the protein environment on energy and charge-transfer excitations. Our calculations show that a forward charge transfer into the A branch is significantly lower in energy than the first charge transfer into the B branch, in agreement with the unidirectional charge transfer observed experimentally. We further show that inclusion of the protein environment redshifts this excitation significantly, allowing for energy transfer from the coupled Q_x excitations. Through analysis of transition and difference densities, we demonstrate that most of the Q -band excitations are strongly delocalized over several pigments and that both their spatial delocalization and charge-transfer character determine how strongly affected they are by thermally-activated molecular vibrations. Our results suggest a mechanism for charge-transfer in this bacterial reaction center and pave the way for further first-principles investigations of the interplay between delocalized excited states, vibronic coupling, and the role of the protein environment of this and other complex light-harvesting systems.

I. INTRODUCTION

In natural photosynthesis the energy of sun light is converted into chemical energy in highly efficient excitation- and charge-transfer processes¹. Absorption of light happens primarily in antenna complexes, which funnel the excitation energy towards the reaction center (RC) where a charge-separation step initiates a cascade of electron-transfer processes resulting in a proton gradient that drives the biochemical reactions of photosynthesis. In purple bacteria such as *Rhodobacter sphaeroides*, the fundamental design principles of these pigment-protein complexes are well understood due to a wealth of experimental and computational techniques that give access to detailed structural and spectroscopic information²⁻⁹. In this respect, the bacterial RC can also be understood as a model system for the RC of more complex photosynthetic organisms because its structure is highly conserved across bacteria, algae, and plants¹⁰. Its main building blocks, shown in Figure 1, are arranged along two pseudosymmetric branches A and B and consist of a strongly coupled dimer of two bacteriochlorophyll (BCL) molecules dubbed the special pair (P), two accessory BCLs (B_A , B_B), two bacteriopheophytines (H_A , H_B), and two quinones (Q_A , Q_B) embedded in a transmembrane protein matrix.

Despite the similar, but not exactly symmetric, structure of the A and B branches, it is well-established that the primary charge separation reaction only proceeds along the A branch with near-unity quantum efficiency¹¹⁻¹³. The ultrafast timescales on which the primary energy- and charge-transfer processes occur in the RC in combination with broad overlapping absorption peaks originating from the coupling of mul-

iple pigments and their protein environments, have posed significant challenges to spectroscopic techniques. Two-dimensional electronic spectroscopy (2DES) has become one of the primary experimental techniques for studying the bacterial RC^{7,14-16} and other photosynthetic systems^{17,18}. For the RC of *Rhodobacter sphaeroides* and similar RCs, 2DES has been used to propose models for the kinetics of the primary charge separation. In these models, it is usually assumed that charge separation is initiated through the excitation of P (denoted as P^*), leading to a charge-transfer intermediate $P_A^+ P_B^-$, which is followed by a charge-separated state $P^+ H_A^-$ via an ultra-shortlived intermediate $P^+ B_A^-$ ^{7,15}, however, alternative charge-separation pathways have been suggested as well, for example starting from an excitation localized on one or both accessory BCLs, i.e., B_A^* or B^* ¹⁹⁻²² (Figure 1).

Computational modelling has played an important role in helping to unravel the intricate factors affecting excitation and charge transfer in the antenna complexes and the RC. Calculations based on model Hamiltonians and advances in the semiempirical modelling of long- and short-range coupling between chromophores have allowed for the simulation of excitation processes in large pigment-protein complexes²³⁻²⁵. However, also computationally more demanding first-principles calculations, primarily based on (time-dependent) density functional theory (TDDFT), have been employed to study systems of growing complexity and size. The focus of many studies has been the origin of the unidirectionality of the charge-separation process in bacterial RCs and photosystem II of plants.

For the RC of photosystem II, a large model system was used by T. Frankcombe including four (truncated) chloro-

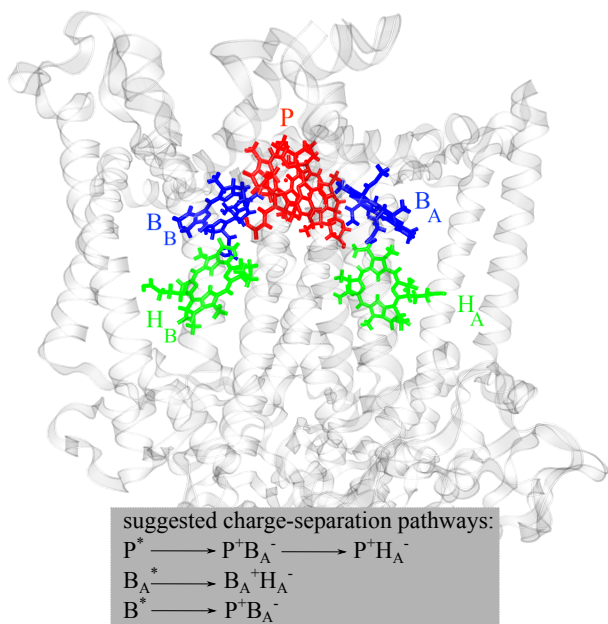


FIG. 1. Proposed charge-separation pathways^{7,15,19–22} and structural model of the RC of *Rhodobacter sphaeroides* including the special pair (P in red), two accessory BCLs (B_A , B_B in blue), and two bacteriopheophytins (H_A , H_B in green). Protein chains are shown in transparent grey. Hydrogen atoms are omitted for clarity.

phyll, two pheophytin, and two plastoquinone molecules using TDDFT and a polarizable continuum model (PCM) to account for effects of the protein environment²⁶. Later, Sirohiwal *et al.* reported TDDFT calculations using a range-separated hybrid functional on chlorophyll monomers, dimers, and trimers of the photosystem II RC showing that the lowest-energy charge-transfer excitation corresponds to $B_A^+H_A^-$ and is strongly affected by protein electrostatics²⁷. Low-energy charge-transfer excitations were also reported by Kavanagh *et al.* in TDDFT calculations using a hexameric model of the photosystem II RC including parts of the protein environment explicitly. Similarly, Förster *et al.* observed an excitation with partial $H_A^-B_A^+$ charge-transfer character using the GW+Bethe-Salpeter Equation approach²⁸.

For the RC of *Rhodobacter sphaeroides*, (TD)DFT calculations including the special pair and some of its neighboring amino-acid residues were reported in 2011 by Wawrzyniak *et al.* and indicated that protein induced distortions of the special pair geometry lead to an asymmetric ground-state electron density²⁹. A similar model system was employed by Eisenmayer *et al.*, who performed molecular dynamics simulations based on constrained DFT and showed that the electron-density asymmetry is dynamical and coupled to a low-frequency vibrational mode, related to the rotation of a histidine residue close to B_A ³⁰. Later, Eisenmayer *et al.* included the B_A in their constrained DFT simulations showing the coupling of proton displacements to the primary electron-transfer step from P to B_A ³¹. Aksu *et al.* combined TDDFT with a tuned range-separated hybrid functional with PCM and showed that spectral asymmetries arise from locally different

dielectric environments along the A and B branches³². The initial charge-transfer excitations of P were also studied by Aksu *et al.* employing the same methodology³³. (TD)DFT calculations by Mitsuhashi *et al.* in which the environment of P together with either B_A or B_B was represented using a QM/MM/PCM scheme, further indicated that the lowest unoccupied molecular orbital (LUMO) of B_A is lower in energy than the LUMO of B_B , suggesting that B_A is the primary electron acceptor³⁴. Another study in which some of the same authors used a diabaticization scheme to evaluate electronic couplings between P and B_A and B_B , respectively, pointed to the particular importance of a tyrosine residue close to B_A as being responsible for the directionality of charge transfer³⁵. Brütting *et al.* investigated the primary charge separation step in the quasi-symmetric reaction center of *Heliobacterium Modesticaldum*, with an emphasis on revealing the influence of nuclear motion on the relative energetic positions of different electronic excitations³⁶.

To the best of our knowledge, explicit TDDFT calculations on a reaction center model of *Rhodobacter sphaeroides* including all six primary pigments and parts of the environment have not been reported yet. Furthermore, while previous studies have provided detailed insight into the effects of the protein environment and molecular vibrations on excited states, little attention has been directed at the delocalized, correlated multi-particle nature of these excitations. One may wonder whether these characteristics can be properly captured by TDDFT, as the wave-functions obtained in TDDFT have no rigorous physical meaning. We here show, however, that one can analyze the excitations reliably based on transition densities and difference densities, i.e., quantities that have a solid foundation in TDDFT.

To this end, we use TDDFT with an optimally-tuned range-separated hybrid functional to study a hexameric model of the RC including the primary pigments, i.e., the special pair P , the accessory BCLs B_A and B_B and the bacteriopheophytins H_A and H_B . We also explicitly model the effect of close-lying amino-acid residues on the excited states by including them in our TDDFT calculations. We clarify which amino acids are responsible for significant changes in excited-state energies and compare our results with QM/MM calculations. Our calculations show that a distinction between localized excitations on the one hand and charge-transfer excitations on the other hand is of limited usefulness to understand the excited state structure of this system of strongly coupled pigments. Instead, we find excitations without charge-transfer character that are delocalized across several pigments and that can not readily be classified as coupled excitations of individual monomeric units. Partial charge-transfer states between the special pair pigments ($P_A^+P_B^-$) are low in energy, mix with these delocalized states and are a consequence of the strong coupling between the pigments. The lowest-energy charge-transfer state that transfers an electron into the A branch can clearly be classified as $B_A^+H_A^-$. This is in agreement with previous first-principles calculations on the photosystem II reaction center, but not in line with experimental reports suggesting charge-transfer through an intermediate $P^+B_A^-$ states. The $B_A^+H_A^-$ excitation is ~ 20 meV higher in energy than the

highest-energy Q -band excitations. Although we cannot rule out that including further parts of the environment might lower its energy further, such a small energetic separation suggests that the vibrational modes of the pigments and/or the environment could couple this charge-transfer state to the delocalized Q -band excitations.

II. COMPUTATIONAL METHODS

A. Structure of Model Systems

All our calculations are based on the experimental crystal structure of the wild-type RC of *Rhodobacter sphaeroides* with Protein Data Bank file ID 1M3X³. The pigment-protein complex has two main protein chains called L- and M-chains which form the backbone of the A and B branches, respectively. We are interested in the primary charge-transfer process and, therefore, included P , B_A , B_B , H_A , and H_B in all our computational models. For approximating the effect of the protein environment on energy- and charge-transfer excitations, we added amino-acid residues explicitly to our model structures, described in more detail in Section III B. Hydrogen atoms are not resolved in the experimental crystal structure and are therefore added with the module HBUILD in CHARMM³⁷ and energetically optimized using the CHARMM force field³⁸ as described in Ref. 39. In all model systems, we cropped the phytyl tails of the BCL molecules and saturated the carboxyl group with a hydrogen atom. Using a methyl group to saturate the phytyl tail does not change the main conclusions of this paper, as shown in Figure S1 of the Supplementary Material (SM). Furthermore, we cut the bonds between the amino-acid residues and the polypeptide chains between C_α and C_β and saturated them with hydrogen atoms.

B. TDDFT Calculations

We performed (TD)DFT calculations using Q-CHEM, version 5.2.2⁴⁰, TURBOMOLE version 7.5^{41,42}, and ORCA version 5.0.2⁴³. We used the Pople basis set 6-31G(d,p) for which the Q_y and Q_x excitation energies of a single BCL a molecule are converged to within 50 meV³⁹. We also tested the accuracy of the basis set for the special pair P as discussed in the SM (Table S1). The exchange-correlation energy is approximated using the optimally-tuned ω PBE functional⁴⁴ which has been shown to properly capture the coupling between BCLs³⁹ and to be *on par* with Green's function-based many-body perturbation theory for a wide range of single chromophores^{45,46}. Range-separated hybrid functionals have also been demonstrated to accurately describe electrochromic shifts due to the protein environment of various biochromophores in an extensive benchmark of DFT approximations by Sirohiwal *et al.*⁴⁷. In the optimally-tuned ω PBE functional, the range-separation parameter determines the length scale at which short-range semilocal exchange goes over into exact long-range exchange. Such functionals significantly improve the description of charge-transfer excitations⁴⁸ and

lead to excellent agreement with experimental photoemission spectroscopy for a broad range of systems from molecules to solids^{49–55}. In the optimal-tuning procedure, the range-separation parameter ω is varied such that the difference between the HOMO eigenvalue ϵ_{HOMO} and the negative ionization potential of both the neutral and the anionic system is minimized⁵⁶. Here, we use $\omega = 0.171a_0^{-1}$ based on tuning for one BCL a performed by Schelter *et al.*³⁹. We confirmed that the deviation of the ionization potentials from $-\epsilon_{HOMO}$ of P and of a single BCL a with coordinating histidine are negligible and do not perform a separate tuning procedure for each of our model systems. This approach is also supported by more general arguments: Using the same ω for each model system allows us to compare the electronic and excited state structure of our model systems on the same footing. Furthermore, optimal tuning of conjugated systems of increasing size leads to artificially low values of ω and, thus, a dominance of semilocal exchange at long range, which deteriorates the description of charge-transfer excitations^{53,57}. For our TDDFT calculations, we used the linear response Casida approach and did not make the Tamm-Dancoff approximation (TDA) unless otherwise noted. We provide further information regarding the numerical convergence of our calculations in the SM. Details of our QM/MM TDDFT calculations with ORCA can also be found in the SM.

C. Classification of Charge-Transfer Excitations

Since the transition density vanishes for charge-transfer states, we calculated the difference density $\Delta n_i = n_i - n_0$ between the excited (n_i) and the ground-state density (n_0) for every excitation i . The excited-state density n_i is calculated as the diagonal part of the excited state density matrix $\gamma^{ii}(r, r') = N \int \Psi^i(r, r_2, r_3, \dots, r_N) \Psi^i(r', r_2, r_3, \dots, r_N) dr_2 \dots dr_N$, where N is the number of electrons and Ψ^i is the generalized Kohn-Sham excited-state wavefunction that consists of a sum of Slater determinants of generalized Kohn-Sham orbitals with coefficients obtained from TDDFT⁵⁸. To quantify the magnitude of charge transfer we integrated over subsystem difference densities. For this purpose, we subdivided the volume containing the difference densities of our full model systems into subsystem volumes, each containing one pigment. Note that P is separated into P_A and P_B , to enable the characterization of internal charge-transfer states of the type $P_A^+ P_B^-$. Our aim is to assign each grid point of the difference-density grid to its closest pigment molecule. For achieving this, we tested two methods for assigning grid points to subsystem volumes: In method 1, we used the distances between grid points and each molecule's atomic coordinates (including hydrogen atoms). In method 2, we used distances between grid points and each molecule's geometrical center of gravity. Both methods result in the same trends, although the absolute values of the integrated subsystem densities differ slightly.

III. RESULTS AND DISCUSSION

A. Absorption Spectrum and Excited State Character of the Bare Hexameric RC Model

We start our discussion by inspecting the absorption spectrum of a hexameric model of the RC based on the crystal structure as described in Section II A and without including any parts of the environment, shown in Figure 2a. For this model, we were able to calculate 16 excitations, corresponding to the energy range depicted in Figure 2a. This energy range is dominated by Q -band excitations, i.e., excited states that originate from the coupling of the Q_y and Q_x excitations of the individual BCL and bacteriopheophytin molecules. However, because of the spatial proximity of these pigments in the RC, not all excitations can clearly be classified as coupled Q_y or Q_x as apparent from their transition densities shown in Figure S2. These transition densities also show that the majority of Q -band excitations is spatially strongly delocalized across several pigments, with some of them spreading over the entire RC model. This is the first main result of our study. A list of excitation energies, oscillator strengths, and spatial character as determined from the transition densities (and difference densities in case of charge-transfer excitations) can be found in Table I. In this Table and in the rest of the text, the notation $(PBH)^*$ corresponds to an excitation delocalized across P , B_A , B_B , H_A , and H_B , while $P_A^+P_B^-$ denotes a charge-transfer excitation from P_A to P_B .

#	Energy	Oscillator Strength	Character
1	1.56	0.83	$(PBH)^*$
2	1.63	0.36	$(PBH_B)^*$
3	1.67	0.33	$(PBH)^*$
4	1.71	0.15	$(PBH)^*$
5	1.80	0.30	$(BH_B)^*$
6	1.84	0.29	$(PB_AH)^*$
7	1.85	0.07	$P_A^+P_B^-$
8	1.92	0.10	$(PBH)^*$
9	2.04	0.18	$(PBH)^*$
10	2.08	0.02	$(P_BBH_B)^*$
11	2.08	0.13	$(PBH)^*$
12	2.09	0.23	$(PBH_A)^*$
13	2.14	0.20	$(PBH_B)^*$
14	2.19	0.02	$P_A^+P_B^-$
15	2.33	0.00	$B_A^+H_A^+$
16	2.34	0.00	$P_A^+P_B^-$

TABLE I. Excitation energies (in eV), oscillator strengths, and spatial delocalization/charge-transfer character of the first 16 excitations of our bare hexameric RC model structure

We find four excitations with charge-transfer character in this energy range. The difference densities of these excitations are depicted in Figure 2b (all other differences densities for this structural model can be found in Figure S3). Here and in the following, positive difference density values indicate a region of space in which the electron density (i.e., negative charge density) increases as a consequence of the excitation (shown in blue), whereas negative values indicate regions of space in which the electron density decreases (shown in red).

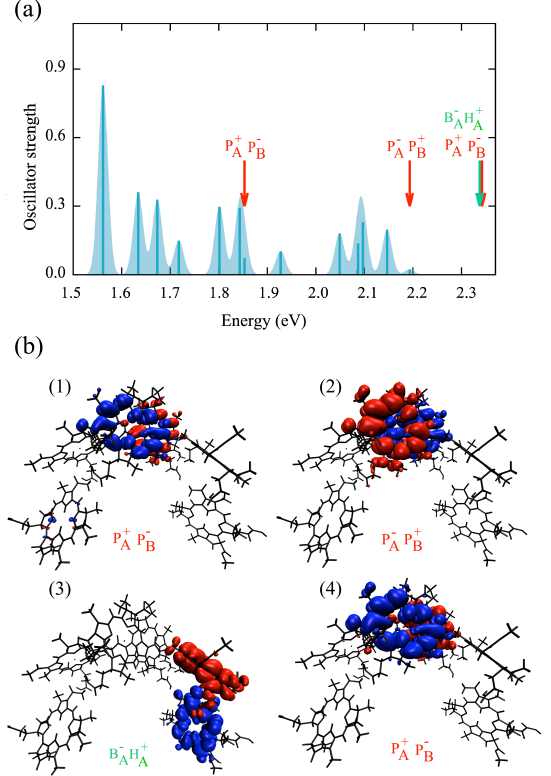


FIG. 2. (a) TDDFT absorption spectrum of the bare hexameric RC model. Arrows mark excitations with low/vanishing oscillator strength and (partial) charge-transfer character. The shaded areas are calculated by folding the excitation energies with Gaussian functions with a width of 0.08 eV as a guide to the eye. (b) Difference densities of the four charge-transfer excitations in this energy range.

Numerical values based on the integration of difference densities as described in Section II C are listed in Table S3. The three charge-transfer excitations within the special pair, corresponding to $P_A^+P_B^-$ and $P_A^-P_B^+$ arise as a consequence of the strong coupling of P_A and P_B . In particular the first $P_A^+P_B^-$ excitation mixes strongly with other excitations at ~ 1.85 eV and therefore exhibits partial charge-transfer character, in which 0.69 of an electron is transferred from P_A to P_B . Strikingly, we also find a charge-transfer excitation from B_A to H_A in this energy range. This is the lowest-energy pure charge-transfer state we find in our calculations (0.99 of an electron is transferred from B_A to H_A). The second main result of our study is that the appearance of this charge-transfer state at ~ 2.3 eV is a consequence of the spatial arrangement of the pigments in the bacterial RC alone. We will discuss how the energy of this state is affected by including environmental effects in Section III C.

B. Effect of the Protein Environment on a Tetrameric RC Model

The importance of the protein environment and its impact on charge transfer were recognized already in early studies

of the bacterial RC^{59–61}. Proposals for how the surrounding proteins affect charge transfer in the RC have primarily included asymmetries in the dielectric environment and in protein electrostatic fields that *A* and *B* branch cofactors experience^{60,62–65}. Our goal here is to include parts of the protein environment explicitly in our TDDFT calculations to elucidate which amino-acid residues electronically couple to the primary RC pigments. For this purpose, we start by studying tetrameric models of the RC including the special pair *P* and the accessory BCLs *B_A* and *B_B*, and systematically increase the number of amino-acid residues in our calculations.

We construct four model systems shown in Figure 3a: Model system *M₁* consists of the four BCL molecules *P_A*, *P_B*, *B_A*, and *B_B*. For a direct analysis of the influence of the closest lying amino acids, the histidine molecules that coordinate each of the BCLs (HIS M202, HIS M182, HIS L173, HIS L153) were included in model system *M₂*. Our largest model system, *M₄*, contains *all* amino acids in a radius of 3 Å around the BCLs. These 32 amino acids were determined by constructing spheres with radius 3 Å around each atom of the four BCL molecules (excluding hydrogen atoms and the phytol tail). A complete list (Table S4) and all structure files can be found in the SM. We calculated the electronic density of states (DOS) of these model systems and found two occupied states localized on amino acids TRP M157 and MET L248, respectively, energetically close to the highest occupied molecular orbital of *M₄* (see Figures S4 and S5). However, a model system *M₃*^{*} consisting of the four primary BCL molecules, the coordinating histidines, and these two amino acids features an electronic DOS distinctly different from that of *M₄* (Figure S6). We therefore additionally included the two main symmetry breaking amino acids PHE M197 and HIS L168 as suggested by Eisenmayer *et al.*³¹ to construct model system *M₃* with a DOS in very good agreement to the DOS of *M₄* in the relevant energy range.

The TDDFT *Q*-band spectra of *M₁* – *M₄* comprising the ten lowest-energy excitations are shown in Figure 3b and Tables S5 and S6. The first four excitations of these model systems can be seen as arising from a coupling of the *Q_y* excitations of *P*, *B_A* and *B_B*. We provide a detailed analysis of the origin of these excitations in the SM (Figures S8 – S10). Inspection of their transition densities (Figure S8) shows that only the first excitation is localized on *P* while excitations 2 to 4 are coupled *Q_y* excitations spread across all four BCLs. Among the following six excitations of *M₁*, 5, 6, and 7 can clearly be assigned to *P*. Two of these excitations (6 and 7) have coupled *Q_x* character; excitation 5 has *Q_y* character but integration over the difference density corresponding to this state also shows substantial charge-transfer character. States 8 and 9 of *M₁* are *Q_x* excitations associated with *B_A* and *B_B*. Excitation 10 of *M₁* is nearly dark and corresponds to a $P_A^+P_B^-$ charge-transfer state.

Inclusion of the histidines in *M₂* hardly affects the first four excitations. Only when further amino-acid residues are added do we observe a noticeable redshift: the first excitation of *M₄* is 40 meV lower in energy than that of *M₁*. The character of these excitations is not changed by the environment.

The average difference density of excitations 1–4 is barely affected by addition of the environment as shown in Figure S11. We observe more significant energy differences for the next six excitations. Excitations with *Q_x* character are redshifted by ~100 meV through addition of the coordinating histidines and the coupled *Q_x* excitations of *P* are redshifted by another 20 meV for model system *M₃*, while the *Q_x* excitations of the accessory BCLs are stable. We note that the significance of the coordinating histidines for these excitations can also be seen in the difference density (Figure S11). In systems *M₂* – *M₄*, there is a clear transfer of positive charge from *P* to the coordinating histidines.

The energy of the (partial) charge-transfer excitations 5 and 10 of *M₁* are also affected by adding the protein environment. Excitation 5 of *M₁* is redshifted by ~60 meV and becomes excitation 6 in *M₄*, and excitation 10 is redshifted by ~100 meV. The magnitude of charge transfer is only slightly affected by the addition of the environment. The amount of charge transferred from *P_A* to *P_B* in excitation 5 of *M₁* decreases slightly when adding the environment while in excitation 10 it remains the same. Overall, the character of excitations 5 to 10 is only slightly affected by the amino-acid environment, as can be seen in Figure S12, which shows the average difference density of excitations 5–10 for systems *M₁* – *M₄*. Importantly, Figure 3b demonstrates that the spectrum of *M₄* is very similar to that of *M₃* with the same order of states and only a small global redshift as compared to *M₃*. We therefore conclude that the eight amino acids considered in *M₃* reproduce the main (static) effects of the amino-acid environment. Therefore, they constitute a "reasonable minimal environment" that should be included explicitly in future calculations.

At energies above the *Q*-band and below the Soret band that starts at ~3 eV¹⁰, we observe a range of dark states with charge-transfer character. Here, we only discuss five states in this energy region that lead to a clear charge transfer between different BCL molecules. The energy and difference densities of these states are shown in Figure 3c. (Integrated) difference densities of all states are shown in Figure S13 and Table S7. Due to the large size of *M₄*, we only calculated twelve excitations with high numerical accuracy for this system. Since the effects of the environment are well-represented by *M₃* as shown before, we do not discuss the charge-transfer excitations of *M₄* in detail. However, Table S5 and S6 show that the energies of the charge-transfer excitations 11 and 12 of *M₃* and *M₄* are in very good agreement.

In similarity to the findings for our hexameric model of the RC, we find a $P_A^-P_B^+$ excitation in *M₁*–*M₃* (excitation 11). Addition of the histidines redshifts this state by 80 meV, while the additional amino acids of *M₃* lead to a blueshift of 26 meV. The 12th excitation corresponds to $P^+B_A^-$. This state is redshifted by 120 meV through the addition of histidines while further amino acids blueshift the excitation back by 110 meV. The energy gap between $P^+B_A^-$ and the next charge-transfer excitation is substantial: ~130 meV in *M₁*, ~210 meV in *M₂* and 85 meV in *M₃*. In the 13th excitation of *M₁*, we observe a backward charge transfer from the B branch corresponding to $P^-B_B^+$. The first forward charge transfer into the B branch ($P^+B_B^-$) occurs at ~2.6 eV, i.e., at significantly higher energies

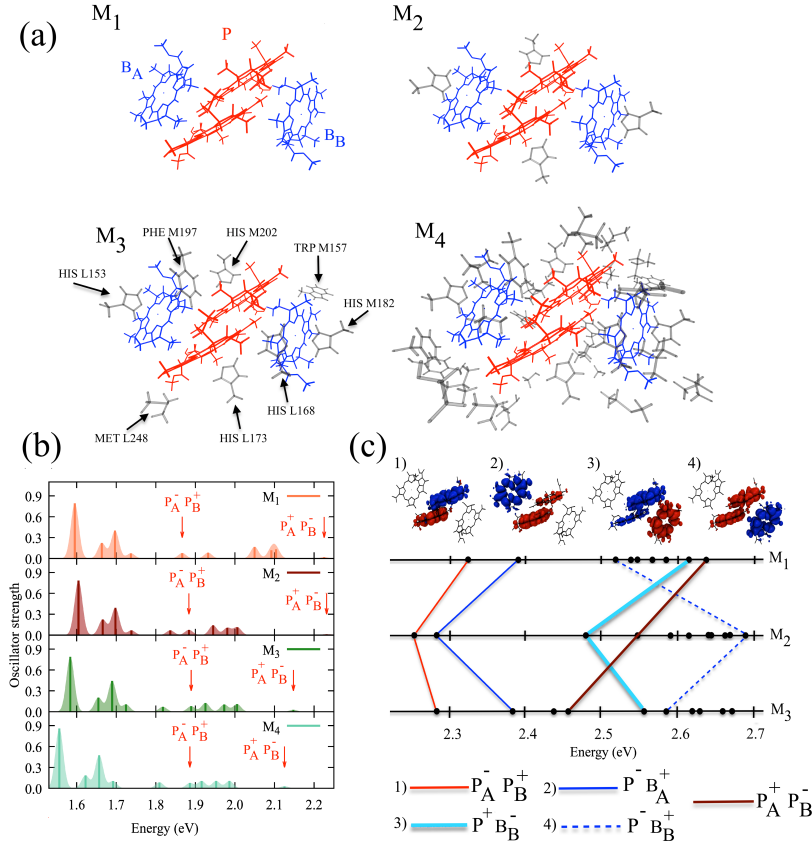


FIG. 3. (a) Representation of model systems M_1 , M_2 , M_3 , and M_4 as described in the main text. (b) Absorption spectra of $M_1 - M_4$ in the energy region where coupled Q_y and Q_x excitations are expected. Red arrows mark excitations with charge-transfer character. (c) Energy of dark excitations (zero oscillator strength) of $M_1 - M_3$ and difference densities of selected charge-transfer excitations of M_1 . The red surface of the difference density shows the isovalue $-0.0001a_0^{-3}$ and the blue surface shows $0.0001a_0^{-3}$.

than $P^+B_A^-$. The addition of amino acids affects this excitation in a similar way as $P^+B_A^-$. These calculations show that inclusion of a (static) protein environment for the system studied here changes excitation energies substantially but hardly affects the character and spatial delocalization of states. For our tetrameric model systems addition of the protein environment also does not lead to a mixing of Q -band excitations and experimentally relevant charge-transfer states.

To approximate the effect of molecular vibrations on the energy of the excited states, we also calculated the normal mode spectrum of model system M_1 in TURBOMOLE using the B3LYP functional and def2-SVP basis set. We then distorted the structure along each of the normal modes with a distortion amplitude corresponding to 300 K, and calculated the TDDFT excitation spectra in QCHEM with ω PBE as before. The high-frequency modes of M_1 correspond to intramolecular vibrations such as C-C and C-H stretch modes, which are not thermally activated and only have a small effect on the energy of the delocalized excitations that we are interested in here. We therefore only calculated the effect of normal mode distortions on excitation energies for wavenumbers below 85 cm^{-1} . Low-frequency modes correspond to intermolecular vibrations that change the orbital overlap between

neighboring BCL molecules and are thus expected to have a more substantial effect on excitation energies of delocalized and charge-transfer excitations⁶⁶.

Our results, shown in Figure S14, confirm this intuitive picture: The first excitation, corresponding to a coupled Q_y excitation of P , exhibits mode-dependent energy changes of up to 20 meV, while excitations 2 – 4 are much less sensitive to these distortions with energy changes of $\lesssim 10$ meV in line with their spatial delocalization across B_A and B_B , which are far apart. A similar observation holds for the coupled Q_x excitations of P , B_A and B_B . On the other hand, excitations with (partial) charge-transfer character between neighboring molecules are highly sensitive to low-frequency vibrations, exhibiting excitation-energy changes of up to 30 meV for charge transfer between P_A and P_B , and up to 50 meV for charge transfer between P and B_A or B_B . These excitation-energy changes can result in both red- and blueshifts, as shown in Figure S14. Nonetheless, our analysis indicates that inclusion of inter- and intramolecular vibrations does not change our overall result that in a tetrameric model of the bacterial RC, charge-transfer excitations into the A-branch are energetically well-separated from the Q -band excitations. This finding is in line with systematic first-principles molecular dynamics simulations of the

RC of the heliobacterium *Heliobacterium modesticaldum* in Ref. 36. While the first A-branch charge-transfer state is at considerably lower energies for that system, thermal vibrations do not significantly change the spectral overlap of the charge-transfer state with the coupled Q_y excitations as compared to the static structural model³⁶.

Finally, we tested whether the inclusion of further parts of the protein environment through a QM/MM scheme would change our main conclusions. Figure S15 and S16 show the full TDDFT spectrum and the TDA spectrum of M_1 with and without the QM/MM environment. Inclusion of the QM/MM environment leads to changes in the absorption spectrum of comparable size as in our explicit model M_4 . In particular, we also observe a redshift of the first charge-transfer excitation of ~ 200 meV. However, the redshift of the coupled Q_y and Q_x excitations due to the protein environment is smaller in the QM/MM model, and some of the detailed changes in the partial and full charge-transfer excitations are also not captured by the MM environment.

C. Effect of Environment on A and B Branch Excited States

Due to the large size of the hexameric model of the RC discussed in Section III A (494 atoms), a TDDFT calculation including the relevant charge-transfer states for a structural model that also includes significant parts of the protein environment as done for the tetrameric model in Section III B is computationally not feasible. The largest hexameric RC model that we could run full TDDFT calculations for includes the coordinating histidines close to P_A , P_B , B_A and B_B (as in M_2) plus two leucines close to H_A and H_B . Table S2 shows that including these amino-acid residues has similar effects as observed in Section III B, but the calculation of more than the first 13 excitations was not feasible for this system.

However, given the large spatial separation between A- and B-branch accessory BCLs and bacteriopheophytins, we can assume that parts of the spectrum of the full RC arise as combinations of A-branch and B-branch excitations, respectively. To test this assumption, we constructed two further structural models A_1 and B_1 , shown in Figure 4a, comprising P , B_A , and H_A for the A branch, and P , B_B and H_B for the B branch, respectively. We compare the excitation spectrum of the hexameric model with that of A_1 and B_1 , respectively, in Figure 4b. As expected, excitations associated with P appear in all three spectra, albeit at different energies (e.g., the first excitation and the charge-transfer states $P_A^-P_B^+$ and $P_A^+P_B^-$). On the other hand, excitations that are localized on the A- or B-branch, can clearly be assigned to either A_1 or B_1 . In particular, in our calculation of the spectrum of A_1 , we find the charge-transfer state $B_A^+H_A^-$ at the same energy (~ 2.3 eV) as in our hexameric model. We can therefore study the effect of adding amino acids to the energy of this and other relevant charge transfer states using our structural models A_1 and B_1 as a starting point.

A comparison of the excitation energies of the relevant charge-transfer states in A- and B-branch is shown in Figure 4c (and listed in Tables S9 and S10). The $B_A^+H_A^-$ state

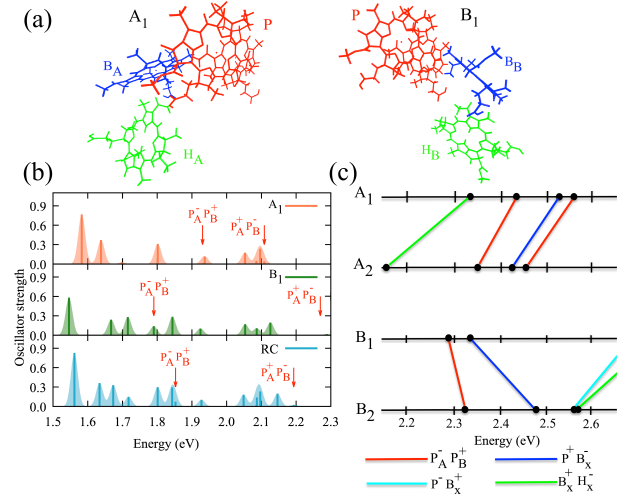


FIG. 4. (a) Structures of model systems A_1 (including $SP+B_A+H_A$) and B_1 including $SP+B_B+H_B$. (b) Absorption spectra of H_{A1} , H_{B1} and RC in the energy region where coupled Q_y and Q_x excitations are expected. Red arrows mark excitations with charge-transfer character. (c) Energy of dark excitations (zero oscillator strength) of $A_1 - A_2$ and $B_1 - B_2$.

is significantly lower in energy than $B_B^+H_B^-$, in agreement with the experimentally observed directionality of charge-separation along the A-branch. By adding the coordinating histidines and leucines in model systems A_2 and B_2 , both states are redshifted by more than 100 meV. Charge-transfer states from P to B_B and P to B_A are significantly higher in energy, in particular after addition of the coordinating histidines and leucines. Adding further amino-acid residues (listed in Table S11), in analogy with M_3 in Section III B, leads to a further redshift of $B_A^+H_A^-$, bringing this charge-transfer state within 25 meV of the coupled Q_x excitations (see Table S9). It is therefore likely that addition of further parts of the protein environment in concert with thermally-activated molecular vibrations could lead to a mixing of this charge-transfer state and the delocalized coupled Q_x excitations.

IV. SUMMARY AND CONCLUSIONS

Our first principles calculations show a pronounced effect of the protein environment on the electronic structure and excited states of the primary six pigments comprising the RC of *Rhodobacter sphaeroides*. By systematically adding relevant amino acids in the vicinity of these chromophores, we find a significant redshift of the coupled Q_y and Q_x excitations. Charge-transfer excitations are observed in the form of dark excitations starting at ~ 0.2 eV above the coupled Q_x excitations. These charge-transfer states are strongly affected by direct inclusion of the protein environment with energy changes of up to ~ 0.2 eV. However, contrary to the coupled Q_y and Q_x excitations, the protein environment affects charge-transfer states of different character differently. In particular, the lowest-energy charge transfer state in our calculations cor-

responds to $B_A^+H_A^-$ and is significantly lower in energy than other excitations that move charge into the A branch. It is also almost 0.5 eV lower than an equivalent excitation in the B-branch. The $B_A^-H_A^+$ excitation is redshifted by the inclusion of close-lying amino-acid residues and can mix with the coupled Q_x excitations.

Beyond suggesting a possible mechanism for charge-transfer in the RC of *Rhodobacter sphaeroides*, our calculations demonstrate the complex excited state landscape of the RC's chromophores. Analysing the transition and differences densities of the excited states allows for several conclusions. While most of the Q -band excitations can be understood as a consequence of the coupling of Q_y and Q_x excitations of the special pair BCLs P and the accessory BCLs B_A and B_B , the close spatial proximity of these molecules leads to strong coupling, mixing in (partial) charge-transfer states of the type $P_A^+P_B^-$ at relatively low energies. Furthermore, only the first high-oscillator strength excitation of the spectrum can be interpreted as a coupled Q_y excitation of the special pair. All other excitations are strongly delocalized, some of them with significant transition density on all six primary pigments. The presence of strongly delocalized excited states corresponding to both energy- and charge-transfer excitations is relevant because delocalized excitations are expected to be more strongly affected by thermally activated molecular vibrations than localized excitations as shown previously by Alvertis *et al.* for the oligo-acene series⁶⁶. In our study we have approximately shown this effect by calculating the exciton renormalization energies of tetrameric model structures distorted along vibrational normal modes. Based on our own calculations and previous literature^{30,31,34,35}, we expect yet more pronounced effects for larger structural models that also include the vibronic coupling to the protein environment.

Finally, our calculations allow us to comment on the interpretation of experimental spectroscopy of pigment-protein complexes like the bacterial RC. Our results suggest that because of the delocalized nature of energy- and charge-transfer excitations in these systems, the assignment of spectroscopic features to linear combinations of localized excitations on individual pigments is not always justified. Care should be taken when modelling the strongly coupled pigments of the bacterial RC in terms of their constituting elements.

SUPPLEMENTARY MATERIAL

Additional convergence data, excitation energies, difference densities and transition densities not shown in the main text, a discussion of the spectral origin of the coupled Q_y and Q_x excitations, details on the QM/MM calculations, results for vibrationally excited structures, and structure files of model systems $M_1 - M_4$ and our bare hexameric model.

ACKNOWLEDGMENTS

This work was supported by the Bavarian State Ministry of Science and the Arts through the Elite Network Bavaria

(ENB), the Collaborative Research Network Solar Technologies go Hybrid (SolTech), the Study Program "Biological Physics" of the ENB, and through computational resources provided by the Bavarian Polymer Institute (BPI).

- ¹G. Renger, "Overview of Primary Processes of Photosynthesis," in *Primary Processes of Photosynthesis*, edited by G. Renger (RSC Publishing, 2008) pp. 5–30.
- ²X. J. Jordanides, G. D. Scholes, and G. R. Fleming, "The mechanism of energy transfer in the bacterial photosynthetic reaction center," *J. Phys. Chem. B* **105**, 1652–1669 (2001).
- ³A. Camara-Artigas, D. Brune, and J. P. Allen, "Interactions between lipids and bacterial reaction centers determined by protein crystallography | PNAS," *Proc. Nat. Aca. Sci.* **99**, 11055–11060 (2002).
- ⁴D. M. Jonas, M. J. Lang, Y. Nagasawa, T. Joo, and G. R. Fleming, "Pump-probe polarization anisotropy study of femtosecond energy transfer within the photosynthetic reaction center of *Rhodobacter sphaeroides* R26," *J. Phys. Chem.* **100**, 12660–12673 (1996).
- ⁵G. S. Schlau-Cohen, E. D. Re, R. J. Cogdell, and G. R. Fleming, "Determination of Excited-State Energies and Dynamics in the B Band of the Bacterial Reaction Center with 2D Electronic Spectroscopy," *J. Phys. Chem. Lett.* **3**, 2487–2492 (2012).
- ⁶O. Rancova, R. Jankowiak, A. Kell, M. Jassas, and D. Abramavicius, "Band Structure of the *Rhodobacter sphaeroides* Photosynthetic Reaction Center from Low-Temperature Absorption and Hole-Burned Spectra," *J. Phys. Chem. B* **120**, 5601–5616 (2016).
- ⁷A. Niedringhaus, V. R. Policht, R. Sechrist, A. Konar, P. D. Laible, D. F. Bocian, D. Holten, C. Kirmaier, and J. P. Ogilvie, "Primary processes in the bacterial reaction center probed by two-dimensional electronic spectroscopy," *Proc. Nat. Acad. Sci.* **115**, 3563–3568 (2018).
- ⁸K. Kawashima and H. Ishikita, "Energetic insights into two electron transfer pathways in light-driven energy-converting enzymes," *Chemical Science* **9**, 4083–4092 (2018).
- ⁹M. A. Kavanagh, J. K. Karlsson, J. D. Colburn, L. M. Barter, and I. R. Gould, "A TDDFT investigation of the photosystem II reaction center: Insights into the precursors to charge separation," *Proc. Nat. Acad. Sci.* **117**, 19705–19712 (2020).
- ¹⁰R. J. Cogdell, A. Gall, and J. Köhler, "The architecture and function of the light-harvesting apparatus of purple bacteria: from single molecules to in vivo membranes," *Quarterly Reviews of Biophysics* **39**, 227–324 (2006).
- ¹¹C. A. Wraight and R. K. Clayton, "The absolute quantum efficiency of bacteriochlorophyll photooxidation in reaction centres of *Rhodospseudomonas sphaeroides*," *Biochimica et Biophysica Acta (BBA) - Bioenergetics* **333**, 246–260 (1974).
- ¹²C. Kirmaier, D. Holten, and W. W. Parson, "Picosecond-photodichroism studies of the transient states in *Rhodospseudomonas sphaeroides* reaction centers at 5 K. Effects of electron transfer on the six bacteriochlorin pigments," *Biochimica et Biophysica Acta (BBA) - Bioenergetics* **810**, 49–61 (1985).
- ¹³W. Zinth and J. Wachtveitl, "The First Picoseconds in Bacterial Photosynthesis—Ultrafast Electron Transfer for the Efficient Conversion of Light Energy," *ChemPhysChem* **6**, 871–880 (2005).
- ¹⁴F. Ma, E. Romero, M. R. Jones, V. I. Novoderezhkin, and R. van Grondelle, "Vibronic Coherence in the Charge Separation Process of the *Rhodobacter sphaeroides* Reaction Center," *J. Phys. Chem. Lett.* **9**, 1827–1832 (2018).
- ¹⁵F. Ma, E. Romero, M. R. Jones, V. I. Novoderezhkin, and R. van Grondelle, "Both electronic and vibrational coherences are involved in primary electron transfer in bacterial reaction center," *Nature Communications* **10** (2019), 10.1038/s41467-019-08751-8.
- ¹⁶V. R. Policht, A. Niedringhaus, R. Willow, P. D. Laible, D. F. Bocian, C. Kirmaier, D. Holten, T. Mančal, and J. P. Ogilvie, "Hidden vibronic and excitonic structure and vibronic coherence transfer in the bacterial reaction center," *Science Advances* **8**, eabk0953 (2022).
- ¹⁷M. Tros, V. I. Novoderezhkin, R. Croce, R. v. Grondelle, and E. Romero, "Complete mapping of energy transfer pathways in the plant light-harvesting complex Lhca4," *Phys. Chem. Chem. Phys.* **22**, 25720–25729 (2020).
- ¹⁸H. H. Nguyen, Y. Song, E. L. Maret, Y. Silori, R. Willow, C. F. Yocum, and J. P. Ogilvie, "Charge Separation in the Photosystem II Reaction Cen-

- ter Resolved by Multispectral Two-Dimensional Electronic Spectroscopy," (2022).
- ¹⁹M. E. van Brederode, J. P. Ridge, I. H. M. van Stokkum, F. van Mourik, M. R. Jones, and R. van Grondelle, "On the efficiency of energy transfer and the different pathways of electron transfer in mutant reaction centers of *Rhodobacter sphaeroides*," *Photosynthesis Research* **55**, 141–146 (1998).
 - ²⁰H. Zhou and S. G. Boxer, "Probing Excited-State Electron Transfer by Resonance Stark Spectroscopy. 1. Experimental Results for Photosynthetic Reaction Centers," *J. Phys. Chem. B* **102**, 9139–9147 (1998).
 - ²¹S. Lin, J. Jackson, A. K. W. Taguchi, and N. W. Woodbury, "Excitation Wavelength Dependent Spectral Evolution in *Rhodobacter sphaeroides* R-26 Reaction Centers at Low Temperatures: The Qy Transition Region," *J. Phys. Chem. B* **102**, 4016–4022 (1998).
 - ²²L. Huang, N. Ponomarenko, G. P. Wiederrecht, and D. M. Tiede, "Cofactor-specific photochemical function resolved by ultrafast spectroscopy in photosynthetic reaction center crystals," *Proc. Nat. Aca. Sci.* **109**, 4851–4856 (2012).
 - ²³M. E.-A. Madjet, F. Müh, and T. Renger, "Deciphering the influence of short-range electronic couplings on optical properties of molecular dimers: Application to "special pairs" in photosynthesis," *J. Phys. Chem. B* **113**, 12603–12614 (2009).
 - ²⁴F. Zheng, M. Jin, T. Mančal, and Y. Zhao, "Study of Electronic Structures and Pigment–Protein Interactions in the Reaction Center of Thermochromatium tepidum with a Dynamic Environment," *J. Phys. Chem. B* **120**, 10046–10058 (2016).
 - ²⁵S. J. Jang and B. Mennucci, "Delocalized excitons in natural light-harvesting complexes," *Rev. Mod. Phys.* **90**, 35003 (2018).
 - ²⁶T. J. Frankcombe, "Explicit calculation of the excited electronic states of the photosystem II reaction centre," *Phys. Chem. Chem. Phys.* **17**, 3295–3302 (2015).
 - ²⁷A. Sirohiwal, F. Neese, and D. A. Pantazis, "Protein Matrix Control of Reaction Center Excitation in Photosystem II," *J. Am. Chem. Soc.* **142**, 18174–18190 (2020).
 - ²⁸A. Förster and L. Visscher, "Quasiparticle Self-Consistent GW-Bethe–Salpeter Equation Calculations for Large Chromophoric Systems," *J. Chem. Theor. Comp.* **18**, 6779–6793 (2022).
 - ²⁹P. K. Wawrzyniak, M. T. Beerepoot, H. J. De Groot, and F. Buda, "Acetyl group orientation modulates the electronic ground-state asymmetry of the special pair in purple bacterial reaction centers," *Phys. Chem. Chem. Phys.* **13**, 10270–10279 (2011).
 - ³⁰T. J. Eisenmayer, H. J. De Groot, E. Van De Wetering, J. Neugebauer, and F. Buda, "Mechanism and reaction coordinate of directional charge separation in bacterial reaction centers," *J. Phys. Chem. Lett.* **3**, 694–697 (2012).
 - ³¹T. J. Eisenmayer, J. A. Lasave, A. Monti, H. J. M. De Groot, and F. Buda, "Proton displacements coupled to primary electron transfer in the *Rhodobacter sphaeroides* reaction center," *J. Phys. Chem. B* **117**, 11162–11168 (2013).
 - ³²H. Aksu, A. Schubert, E. Geva, and B. D. Dunietz, "Explaining Spectral Asymmetries and Excitonic Characters of the Core Pigment Pairs in the Bacterial Reaction Center Using a Screened Range-Separated Hybrid Functional," *J. Phys. Chem. B* **123**, 8970–8975 (2019).
 - ³³H. Aksu, A. Schubert, S. Bhandari, A. Yamada, E. Geva, and B. D. Dunietz, "On the Role of the Special Pair in Photosystems as a Charge Transfer Rectifier," *J. Phys. Chem. B* **124**, 1987–1994 (2020).
 - ³⁴K. Mitsuhashi, H. Tamura, K. Saito, and H. Ishikita, "Nature of Asymmetric Electron Transfer in the Symmetric Pathways of Photosystem i," *J. Phys. Chem. B* **125**, 2879–2885 (2021).
 - ³⁵H. Tamura, K. Saito, and H. Ishikita, "The origin of unidirectional charge separation in photosynthetic reaction centers: nonadiabatic quantum dynamics of exciton and charge in pigment-protein complexes," *Chem. Sci.* **12**, 8131–8140 (2021).
 - ³⁶M. Brütting, J. M. Foerster, and S. Kümmel, "Investigating Primary Charge Separation in the Reaction Center of *Heliobacterium modesticaldum*," *J. Phys. Chem. B* **125**, 3468–3475 (2021).
 - ³⁷B. R. Brooks, C. L. Brooks III, A. D. Mackerell Jr., L. Nilsson, R. J. Petrella, B. Roux, Y. Won, G. Archontis, C. Bartels, S. Boresch, A. Cafilisch, L. Caves, Q. Cui, A. R. Dinner, M. Feig, S. Fischer, J. Gao, M. Hodoscek, W. Im, K. Kuczera, T. Lazaridis, J. Ma, V. Ovchinnikov, E. Paci, R. W. Pastor, C. B. Post, J. Z. Pu, M. Schaefer, B. Tidor, R. M. Venable, H. L. Woodcock, X. Wu, W. Yang, D. M. York, and M. Karplus, "Charmm: The biomolecular simulation program," *J. Comp. Chem.* **30**, 1545–1614 (2009).
 - ³⁸A. D. MacKerell Jr., C. L. Brooks III, L. Nilsson, B. Roux, Y. Won, and M. Karplus, "Charmm: The energy function and its parameterization with an overview of the program," (John Wiley & Sons: Chichester, 1998) pp. 271–277.
 - ³⁹I. Schelter, J. M. Foerster, A. T. Gardiner, A. W. Roszak, R. J. Cogdell, G. M. Ullmann, T. B. De Queiroz, S. Kümmel, A. T. Gardiner, R. J. Cogdell, M. Ullmann, B. D. Queiroz, and S. Kümmel, "Assessing Density Functional Theory in real-time and real-space as a tool for studying bacteriochlorophylls and the light-harvesting complex 2," *J. Chem. Phys.* **151**, 134114 (2019).
 - ⁴⁰Y. Shao, Z. Gan, E. Epifanovsky, A. T. Gilbert, M. Wormit, J. Kussmann, A. W. Lange, A. Behn, J. Deng, X. Feng, D. Ghosh, M. Goldey, P. R. Horn, L. D. Jacobson, I. Kaliman, R. Z. Khaliullin, T. Kus, A. Landau, J. Liu, E. I. Proynov, Y. M. Rhee, R. M. Richard, M. A. Rohrdanz, R. P. Steele, E. J. Sundstrom, H. L. Woodcock, P. M. Zimmerman, D. Zuev, B. Albrecht, E. Alguire, B. Austin, G. J. Beran, Y. A. Bernard, E. Berquist, K. Brandhorst, K. B. Bravaya, S. T. Brown, D. Casanova, C. M. Chang, Y. Chen, S. H. Chien, K. D. Closser, D. L. Crittenden, M. Diedenhofen, R. A. Distasio, H. Do, A. D. Dutoi, R. G. Edgar, S. Fatehi, L. Fusti-Molnar, A. Ghysels, A. Golubeva-Zadorozhnyaya, J. Gomes, M. W. Hantsch-Heine, P. H. Harbach, A. W. Hauser, E. G. Hohenstein, Z. C. Holden, T. C. Jagau, H. Ji, B. Kaduk, K. Khistyayev, J. Kim, J. Kim, R. A. King, P. Klunzinger, D. Kosenkov, T. Kowalczyk, C. M. Krauter, K. U. Lao, A. D. Laurent, K. V. Lawler, S. V. Levchenko, C. Y. Lin, F. Liu, E. Livshits, R. C. Lochan, A. Luenser, P. Manohar, S. F. Manzer, S. P. Mao, N. Mardirossian, A. V. Marenich, S. A. Maurer, N. J. Mayhall, E. Neuscamman, C. M. Oana, R. Olivares-Amaya, D. P. O'Neill, J. A. Parkhill, T. M. Perrine, R. Peverati, A. Prociuk, D. R. Rehn, E. Rosta, N. J. Russ, S. M. Sharada, S. Sharma, D. W. Small, A. Sodt, T. Stein, D. Stück, Y. C. Su, A. J. Thom, T. Tsuchimochi, V. Vanovschi, L. Vogt, O. Vydrov, T. Wang, M. A. Watson, J. Wenzel, A. White, C. F. Williams, J. Yang, S. Yeganeh, S. R. Yost, Z. Q. You, I. Y. Zhang, C. Zhang, Y. Zhao, B. R. Brooks, G. K. Chan, D. M. Chipman, C. J. Cramer, W. A. Goddard, M. S. Gordon, W. J. Hehre, A. Klamt, H. F. Schaefer, M. W. Schmidt, C. D. Sherrill, D. G. Truhlar, A. Warshel, X. Xu, A. Aspuru-Guzik, R. Baer, A. T. Bell, N. A. Besley, J. D. Chai, A. Dreuw, B. D. Dunietz, T. R. Furlani, S. R. Gwaltney, C. P. Hsu, Y. Jung, J. Kong, D. S. Lambrecht, W. Liang, C. Ochsenfeld, V. A. Rassolov, L. V. Slipchenko, J. E. Subotnik, T. Van Voorhis, J. M. Herbert, A. I. Krylov, P. M. Gill, and M. Head-Gordon, "Advances in molecular quantum chemistry contained in the Q-Chem 4 program package," *Molec. Phys.* **113**, 184–215 (2015).
 - ⁴¹"Turbomole V7.5 2020, a development of University of Karlsruhe and Forschungszentrum Karlsruhe GmbH, 1989-2007, TURBOMOLE GmbH since 2007; available from <https://www.turbomole.org>."
 - ⁴²S. G. Balasubramani, G. P. Chen, S. Coriani, M. Diedenhofen, M. S. Frank, Y. J. Franzke, F. Furche, R. Grotjahn, M. E. Harding, C. Hättig, A. Hellweg, B. Helmich-Paris, C. Holzer, U. Huniar, M. Kaupp, A. Marefat Khah, S. Karbalaei Khani, T. Müller, F. Mack, B. D. Nguyen, S. M. Parker, E. Perl, D. Rappoport, K. Reiter, S. Roy, M. Rückert, G. Schmitz, M. Sierka, E. Tapavicza, D. P. Tew, C. van Wüllen, V. K. Voora, F. Weigend, A. Wodyński, and J. M. Yu, "TURBOMOLE: Modular program suite for ab initio quantum-chemical and condensed-matter simulations," *J. Chem. Phys.* **152**, 184107 (2020).
 - ⁴³F. Neese, "The ORCA program system," *WIREs Comput. Mol. Sci.* **2**, 73–78 (2012).
 - ⁴⁴O. a. Vydrov, J. Heyd, A. V. Krukau, and G. E. Scuseria, "Importance of short-range versus long-range Hartree-Fock exchange for the performance of hybrid density functionals," *J. Chem. Phys.* **125**, 074106 (2006).
 - ⁴⁵T. B. De Queiroz, E. R. De Figueroa, M. Coutinho-Neto, C. D. Maciel, E. Tapavicza, Z. Hashemi, and L. Leppert, "First principles theoretical spectroscopy of Methylene Blue: Between limitations of time-dependent density functional theory approximations and its realistic description in the solvent," *J. Chem. Phys.* **154**, 044106 (2021).
 - ⁴⁶Z. Hashemi and L. Leppert, "Assessment of the ab initio Bethe-Salpeter equation approach for the low-lying excitation energies of bacteriochlorophylls and chlorophylls," *J. Phys. Chem. A* **125**, 2163–2172 (2021).
 - ⁴⁷A. Sirohiwal, F. Neese, and D. A. Pantazis, "How Can We Predict Accurate Electrochromic Shifts for Biochromophores? A Case Study on the Photosynthetic Reaction Center," *J. Chem. Theor. Comput.* **17**, 1858–1873 (2017).

- (2021).
- ⁴⁸S. Kümmel, “Charge-Transfer Excitations: A Challenge for Time-Dependent Density Functional Theory That Has Been Met,” *Adv. Energy Mater.* **7**, 1700440 (2017).
 - ⁴⁹S. Refaely-Abramson, R. Baer, and L. Kronik, “Fundamental and excitation gaps in molecules of relevance for organic photovoltaics from an optimally tuned range-separated hybrid functional,” *Phys. Rev. B* **84**, 075144 (2011).
 - ⁵⁰S. Refaely-Abramson, S. Sharifzadeh, N. Govind, J. Autschbach, J. B. Neaton, R. Baer, and L. Kronik, “Quasiparticle Spectra from a Nonempirical Optimally Tuned Range-Separated Hybrid Density Functional,” *Phys. Rev. Lett.* **109**, 226405 (2012).
 - ⁵¹T. Körzdörfer and N. Marom, “Strategy for finding a reliable starting point for G_0W_0 demonstrated for molecules,” *Phys. Rev. B* **86**, 041110 (2012).
 - ⁵²S. Refaely-Abramson, S. Sharifzadeh, M. Jain, R. Baer, J. B. Neaton, and L. Kronik, “Gap renormalization of molecular crystals from density-functional theory,” *Phys. Rev. B* **88**, 081204 (2013).
 - ⁵³T. B. De Queiroz and S. Kümmel, “Charge-transfer excitations in low-gap systems under the influence of solvation and conformational disorder: Exploring range-separation tuning,” *J. Chem. Phys.* **141**, 084303 (2014).
 - ⁵⁴A. K. Manna, S. Refaely-Abramson, A. M. Reilly, A. Tkatchenko, J. B. Neaton, and L. Kronik, “Quantitative Prediction of Optical Absorption in Molecular Solids from an Optimally Tuned Screened Range-Separated Hybrid Functional,” *J. Chem. Theor. Comp.* **14**, 2919–2929 (2018).
 - ⁵⁵D. Wing, G. Ohad, J. B. Haber, M. R. Filip, S. E. Gant, J. B. Neaton, and L. Kronik, “Band gaps of crystalline solids from Wannier-localization based optimal tuning of a screened range-separated hybrid functional,” *Proc. Nat. Acad. Sci.* **118**, e2104556118 (2020).
 - ⁵⁶L. Kronik, T. Stein, S. Refaely-Abramson, and R. Baer, “Excitation Gaps of Finite-Sized Systems from Optimally Tuned Range-Separated Hybrid Functionals,” *J. Chem. Theory Comp.* **8**, 1515–1531 (2012).
 - ⁵⁷T. Körzdörfer, J. S. Sears, C. Sutton, and J. L. Brédas, “Long-range corrected hybrid functionals for pi-conjugated systems: Dependence of the range-separation parameter on conjugation length,” *J. Chem. Phys.* **135**, 204107 (2011).
 - ⁵⁸F. Plasser, M. Wormit, and A. Dreuw, “New tools for the systematic analysis and visualization of electronic excitations. I. Formalism,” *J. Chem. Phys.* **141**, 024106 (2014).
 - ⁵⁹R. J. Stanley, B. King, and S. G. Boxer, “Excited state energy transfer pathways in photosynthetic reaction centers. 1. Structural symmetry effects,” *J. Phys. Chem.* **100**, 12052–12059 (1996).
 - ⁶⁰M. A. Steffen, K. Lao, and S. G. Boxer, “Dielectric asymmetry in the photosynthetic reaction center,” *Science* **264**, 810–816 (1994).
 - ⁶¹M. Hiyama and N. Koga, “Theoretical study of electron transfer in rhodobacter sphaeroides reaction center,” *Photochem. Photobiol.* **87**, 1297–1307 (2011).
 - ⁶²D. J. Lockhart, C. Kirmaier, D. Holten, and S. G. Boxer, “Electric field effects on the initial electron-transfer kinetics in bacterial photosynthetic reaction centers,” *J. Chem. Phys.* **94**, 6987–6995 (1990).
 - ⁶³R. G. Alden, W. W. Parson, Z. T. Chu, and A. Warshel, “Calculations of Electrostatic Energies in Photosynthetic Reaction Centers,” *J. Am. Chem. Soc.*, 12284–12298 (1995).
 - ⁶⁴M. R. Gunner, A. Nicholls, and B. Honig, “Electrostatic potentials in Rhodopseudomonas viridis reaction centers: Implications for the driving force and directionality of electron transfer,” *J. Phys. Chem.* **100**, 4277–4291 (1996).
 - ⁶⁵M. Saggiu, S. D. Fried, and S. G. Boxer, “Local and global electric field asymmetry in photosynthetic reaction centers,” *J. Phys. Chem. B* **123**, 1527–1536 (2019).
 - ⁶⁶A. M. Alvertis, R. Pandya, L. A. Muscarella, N. Sawhney, M. Nguyen, B. Ehrler, A. Rao, R. H. Friend, A. W. Chin, and B. Monserrat, “Impact of exciton delocalization on exciton-vibration interactions in organic semiconductors,” *Phys. Rev. B* **102**, 081122 (2020).